frontiers | Frontiers in Materials

ORIGINAL RESEARCH
published: 02 June 2022
doi: 10.3389/fmats.2022.896516

3D-Printing Assisted SF-SA Based MgP Hybrid Hydrogel Scaffold for Bone Tissue Engineering

*Qiuyi Mao, Bowen Zhu, Hai Zhuang and Shoushan Bu**

Department of Stomatology, First Affiliated Hospital of Nanjing Medical University, Nanjing, China

A new prototype of hybrid silk fibroin and sodium alginate (SF-SA) based osteogenic hydrogel scaffold with a concentration of 2.5% magnesium phosphate (MgP) based gel was prepared with the assistance of an extrusion-based three-dimensional (3D) printing machine in this study. To determine the optimum ratio of MgP-based gel in the hydrogel, a series of physical and biochemical experiments were performed to determine the proper concentration of MgP in two-dimensional hydrogel films, as well as the cell compatibility with these materials in sequence. The SF-SA hydrogel with 2.5wt% magnesium phosphate (SF-SA/MgP) stood out and then was used to fabricate 3D hydrogel scaffolds according to the consequences of the experiments, with SF-SA hydrogel as a control. Then the morphology and osteogenic activity of the scaffolds were further characterized by field emission scanning electron microscope (SEM), calcium mineralization staining, and reverse transcription-polymerase chain reaction (rt-PCR). The SF-SA/MgP hydrogel scaffold promoted the adhesion of rat mesenchymal stem cells with higher degrees of efficiency under dynamic culture conditions. After co-culturing in an osteogenic differentiation medium, cells seeded on SF-SA/MgP hydrogel scaffold were shown to have better performance on osteogenesis in the early stage than the control group. This work illustrates that the 3D structures of hybrid SF-SA/MgP hydrogel are promising headstones for osteogenic tissue engineering.

Keywords: 3D-printing, hydrogel scaffold, silk fibroin, magnesium phosphate, bone tissue engineering

OPEN ACCESS

Edited by:
Chen Yang,
Wenzhou Institute, University of Chinese Academy of Sciences, China

Reviewed by:
Yingji Mao,
Bengbu Medical College, China
Akalabya Bissoyi,
University of Warwick, United Kingdom

****Correspondence:***
Shoushan Bu
bushsh@vip.sina.com

Specialty section:
This article was submitted to Biomaterials, a section of the journal Frontiers in Materials

Received: *21 March 2022*
Accepted: *22 April 2022*
Published: *02 June 2022*

Citation:
Mao Q, Zhu B, Zhuang H and Bu S (2022) 3D-Printing Assisted SF-SA Based MgP Hybrid Hydrogel Scaffold for Bone Tissue Engineering. Front. Mater. 9:896516. doi: 10.3389/fmats.2022.896516

1 INTRODUCTION

The application of additive manufacture (3D printing technology) has revolutionized bone tissue engineering due to its remarkable ability in simulating tissues by producing precise layer-by-layer deposition of bioactive and biocompatible materials (Murphy and Atala, 2014; Markstedt et al., 2015; Daly et al., 2016a; Groll et al., 2016). This advanced technology has helped to establish models of tumor, drug-releasing, and organ grafts since it was first introduced in 1998 (Kim et al., 1998). Key to the successful application of 3D-printing technology in bone tissue engineering is an appropriate selection of ink based on the working mode of the 3D printing machine such as drops inkjet (Saunders and Derby, 2014), micro-valve dispensing (Gudapati et al., 2016), laser-assisted techniques (Sorkio et al., 2018), and continuous micro-extrusion (Ozbolat and Hospodiuk, 2016). As the most frequently used mode used in bone tissue engineering, extrusion-based printing products show excellent performance on versatility, multiple modes of solidification, and towel adaptation in printing complex structures (Ozbolat and Hospodiuk, 2016; Placone and Engler, 2018). An applicable bioactive ink should be well extrudable to prevent blockage and able to produce 3D

structures with high shape fidelity and mechanical stability. An appropriate bioactive ink should also behave like the extracellular matrix: it can protect cells, provide a stable environment, and subsequently promote the functional expression of cells (Parak et al., 2019). Although many investigations have been conducted by other researchers, an applicable single-component hydrogel with multiple features to greatly fit extrusion-based 3D printing machines has not been achieved (Zhang et al., 2014; Pei et al., 2016; Du et al., 2019).

During the process of optimizing cellular function and tissue integration, the bioactivity of bioink is a critical factor as it is crucial to the creation of a microenvironment similar to extracellular matrix (ECM) in bone. The bioactivity of current hydrogel-based bioinks needs to be improved in cell biocompatibility and bioactivity (adhesion and proliferation), hydrophilicity, osteoconductivity, and osteoinductivity (Ma et al., 2018). One promising approach is to blend inorganic bioactive components with organic matrices, which has been widely used in tissue engineering in recent years (Laurenti et al., 2016).

Silk fibroin (SF), natural polymeric fibrin consisting of 18 amino acids (Palcone et al., 2018; Parak et al., 2019) derived from *Bombyx mori* cocoons, has excellent mechanical properties, biocompatibility, and biodegradability (Du et al., 2019). The applications of SF in biomedicine and 3D printing have been extensively reported in recent years (Wang et al., 2008; Cao and Wang, 2009; Jiang et al., 2009; Shi et al., 2017; Zhong et al., 2019). The featured gelation process of the SF solution would take place under specified conditions on account of the conformational transitions during which the SF molecule chain transfers from random coil to β-sheet (Wang et al., 2008). Among those conditions, Polyethylene glycol (PEG) gelated SF hydrogel was successfully applied as an injectable tissue repair material in a recent study (Wang et al., 2015). However, pure SF gelation was shown to lack osteogenic activity *in vivo* (Zhang et al., 2011), and the natural fibroin is difficult to degrade because of its special crystallization and orientation, as well as compact structure (Cao and Wang, 2009).

Sodium alginate, which was extracted from native brown seaweed (Phaeophyceae) and composed of two uronic acids, β (1–4) linked D-mannuronic acid (M) and α (1–4) linked L-guluronic acid (G) (Lee and Mooney, 2012; Venkatesan et al., 2015), was shown to be another prominent biopolymer for the fabrication of hydrogels (de Moraes et al., 2014; Gong et al., 2016). SA has been widely used as a kind of biomaterial for biomedical applications not only because SA regulates the biodegradation of SF (Zheng et al., 2018; Wang et al., 2020) but also because it helps stabilize organization on the surface to maintain inner stability when exposed to calcium chloride (Smrdel et al., 2006).

In this study, we novelty prepared multiple crosslinking hydrogels with inorganic material magnesium phosphate-based gels. Magnesium phosphate is considered a potential solution to promoting the osteogenic activity function of the hydrogel. Indeed, in recent years, magnesium phosphate (Klammert et al., 2011; Mestres and Ginebra, 2011; Babaie et al., 2016; Babaie et al., 2017) has captured more attention as an alternative for bone replacement. As highlighted by Ostrowski et al. (2016) and Nabiyouni et al. (2018), many MgP phases, such as struvite ($MgNH_4PO_46H_2O$) or newberyite ($MgHPO_43H_2O$) have advantages of better solubility and smaller tendency while transforming into lower soluble phases *in vivo* (Tamimi et al., 2011), since Mg^{2+} ions suppress Hydroxyapatite formation by stabilizing gel-like amorphous calcium phosphate phases to inhibit crystal growth (Yang et al., 2011). This inhibition leads to faster resorption and is likely to pronounce bone regeneration capacity, which has already been demonstrated in a couple of studies carried out in small animal models (Kanter et al., 2018). However, a notable weakness of magnesium phosphate as a blended material applied in extrusion-based 3D printing machines is the clogging of particles that may lead to blockage during extrusion. Previous research has proposed a potential solution to overcoming this—the novel thixotropic magnesium phosphate-based gel (TMP-BG) for 3D bioprinting (Laurenti et al., 2016; Chen et al., 2020). TMP-BG was shown to have excellent printability (Chen et al., 2018).

To optimize the performance of the composites, a new type of 3D-print assisted hybrid SF-SA/MgP hydrogel scaffold was prepared in this study. To adequately utilize the advantages of the composites in hydrogel and minimize their shortages simultaneously, formulations were adjusted and MgP concentration was made in different ratios. Next, the mechanical properties, rheological, bioactivity, *in vitro* behaviors, and printability were characterized and optimized. Then living cells were co-cultured with the hybrid hydrogel scaffolds. Their viability and osteogenic differentiation ability in printed constructs were evaluated. The hybrid mechanisms of the hydrogel scaffolds were also explored in this step.

The objective was to find an alternative scaffold with the assistance of 3D printing technology that promotes osteodifferentation in the early stage and matches degradation with new bone deposition. To achieve the goal, a new prototype of hybrid hydrogel consisting of sodium alginate and MgP-based gel in PEG-gelated silk fibroin hydrogel was created to strengthen the mechanical properties of hydrogel and balance the degradation rate with the newly formed tissues. Previous studies have demonstrated that pore size and the 3D spatial structure of the scaffolds are key factors for cell proliferation, differentiation, and extracellular matrix (ECM) production during bone regeneration (Gudapati et al., 2016; Ma et al., 2018). It has been shown that in bone repair, cells prefer scaffolds with pore sizes between 100 and 300 μm for better proliferation, differentiation, and ECM production ability (Ma et al., 2018). Hence, a 3D-printing hydrogel scaffold with macropores around 200 μm was highly preferred in our study.

2 MATERIALS AND METHODS

2.1 Materials

Silk fibroin was used as the fundamental component of the scaffolds. Thixotropic magnesium phosphate-based gel was made of magnesium hydroxide, sodium hydroxide, and phosphoric acid (Huge, Shanghai). The hydrogels were cross-

TABLE 1 | Formulations of SF-SA/MgP hybrid bioinks.

Formulations	Silk Fibroin (%w/v)	Mg (%w/v)	SA (%w/v)	pH
Mg0	5.0	0	0.5	7.75
Mg1	5.0	1.0	0.5	7.58
Mg2.5	5.0	2.5	0.5	7.63
Mg3	5.0	3	0.5	7.70

linked using PEG-400 (Aladdin, Shanghai), sodium alginate (Macklin, Shanghai), and calcium chloride (Huge, Shanghai).

2.2 Experimental Methods

2.2.1 Preparation of the Silk Fibroin and Sodium Alginate and SF-SA/MgP Hydrogel 2D Films

Silk fibroin/sodium alginate solution was made with a mass of 1 g lyophilized silk fibroin protein particles (Simatech, China) in a volume of 10 ml 0.5% sodium alginate solution. The bioactive nano inorganic MgP hydrogel material was made based on a previous report (Chen et al., 2020). Specifically, the molar ratios of $NaOH/H_3PO_4/Mg(OH)_2$ were 2.87/2/1. The solution and MgP-based gel were mixed in different ratios (**Table 1**), and the acquired liquid was termed M0, M1, M2.5, and M3, in which the concentrations of magnesium phosphate were 0%, 1%, 2.5%, and 3%, respectively. Then the different ratios of mixed solution were quickly and intensely stirred to form a homogeneous slurry. The formulations of SF-SA and SF-SA/MgP gels were optimized experimentally based on the gelation properties. We found that the hydrogel would collapse when the concentration of MgP was over 5%. Afterward, an equivalent volume of 80% PEG-400 was added to facilitate the gelation of silk fibroin. The solvent was added to separate wells of a 24-well-plate at a volume sufficient to coat the base of the well before its gelation at 37°C. The 0.2M $CaCl_2$ solution was added to each well to make SA crosslink with Ca^{2+} to obtain a firmer surface before the next step. Then all the wells were washed three times with ddH_2O and PBS in turn to exclude PEG and Cl^- ions and were sterilized by 30 min exposure to UV light in a biological safety cabinet. Plates were either seeded with cells immediately or stored at 4°C until use. Moreover, SF-SA hydrogel was prepared as a control.

2.2.2 Spectroscopic Characterization

Fourier transform infrared (FT-IR) spectroscopy was carried out to have a better understanding of the properties of individual materials. The spectra of Lyophilized SF-SA/MgP hydrogels and SF-SA hydrogel, collected from wavelength 4,000 to 400 cm^{-1} with a resolution of 4 cm^{-1} were analyzed by using an FT-IR spectrometer (IN10, Thermo Scientific).

2.2.3 Rheological Characterization

Rheological measurements were carried out on a Rotational Rheometer (Thermo HAAKE MARS60) at room temperature. The samples were all reached into a state of equilibrium for 60 s before measurement. A parallel plate (35 mm) was used for the four formulated inks, and the shear viscosity was measured at shear rates from 0.01 to 1,000 s^{-1}. A pressure of 10 Pa was chosen for the oscillation frequency measurements conducted at a frequency range of 10^{-1}–10 Hz. The 100s^{-1} shear rate was estimated to be the maximum shear rate experienced by the SF-SA-based hydrogels during the 3D printing process.

2.2.4 *In vitro* Cellular Activities

2.2.4.1 Rat Bone Mesenchymal Stem Cell Isolation and Culture

Rat BMSCs were extracted from the bone marrow of 4-week-old Sprague–Dawley rats (Nanjing Medical University Experimental Animal Center, China). All experiments related to the use of animals were approved by the Institutional Animal Care and Use Committee, following the procedure for Animal Experimental Ethical Inspection of Jiangsu Province Hospital, which is affiliated with Nanjing Medical University. In accordance with previous research (Jiang et al., 2009), the rats were euthanized by the injection of overdosed 10% chloral hydrate. Then the femurs were cut off and separated into pieces at the epiphysis, and the bone marrow was quickly rinsed using PBS supplemented with 2% streptomycin and penicillin. The harvested cells were incubated in Mesenchymal Stem Cell Medium (MSCM) supplemented with 15% FBS, 100 U/mL streptomycin, and 100 U/mL penicillin at 37°C in an atmosphere containing 5% CO_2. The growth medium was refreshed every 3 days.

2.2.4.2 Assessment of Cell Proliferation and Viability

A CCK-8 assay (n = 3) (Cell Proliferation Kit; Dojindo Laboratories, Japan) was conducted to evaluate cell proliferation on hybrid hydrogels and cytotoxicity. For the CCK-8 assay, the cell-seeded hydrogels were incubated in a 24-well plate (5×10^4 cell/well) in Dulbecco's modified eagle's medium (DMEM) supplemented with 10% FBS, 100 U/mL streptomycin and 100 U/mL penicillin while pure BMSCs was set as control. At different time points of co-culture (1, 3, 5, and 7 days) after cell-seeding on the hydrogels, the wells were switched with fresh medium (300 μL) and then the cck-8 solution (30 μL) was added to incubate for 2.5 h. The optical density at 450 nm absorbance was measured by using a microplate reader after a 100 μL volume of supernatant was added to a new 96-well plate.

2.2.4.3 Cell Adhesion and Morphology

The analysis of cell adhesion and morphology on scaffolds was performed by nuclei staining with F-actin with phalloidin (Actin-Tracker Red-594, Beyotime Biotechnology, China) and fixed in Antifade Mounting Medium with DAPI (P0131, Beyotime Biotechnology, China). Specifically, BMSCs (passage 3) seeded on hydrogel films in a 24-well plate (2×10^4 cells/well) were fixed with 4% paraformaldehyde (Biosharp Life Sciences, China) for at least 30 min and washed with PBS on day 3 and day 7. Cytoskeletal actin filaments were stained with FITC-phalloidin at 1/80 dilution (200 T/ml) in PBS and incubated for 1 h at 37°C, followed by three times PBS washing. The nuclei staining was carried out by incubation for 3 min at room temperature with DAPI. The whole staining procedure should be protected from light. Finally, the samples (n = 3) were observed by fluorescence microscopy.

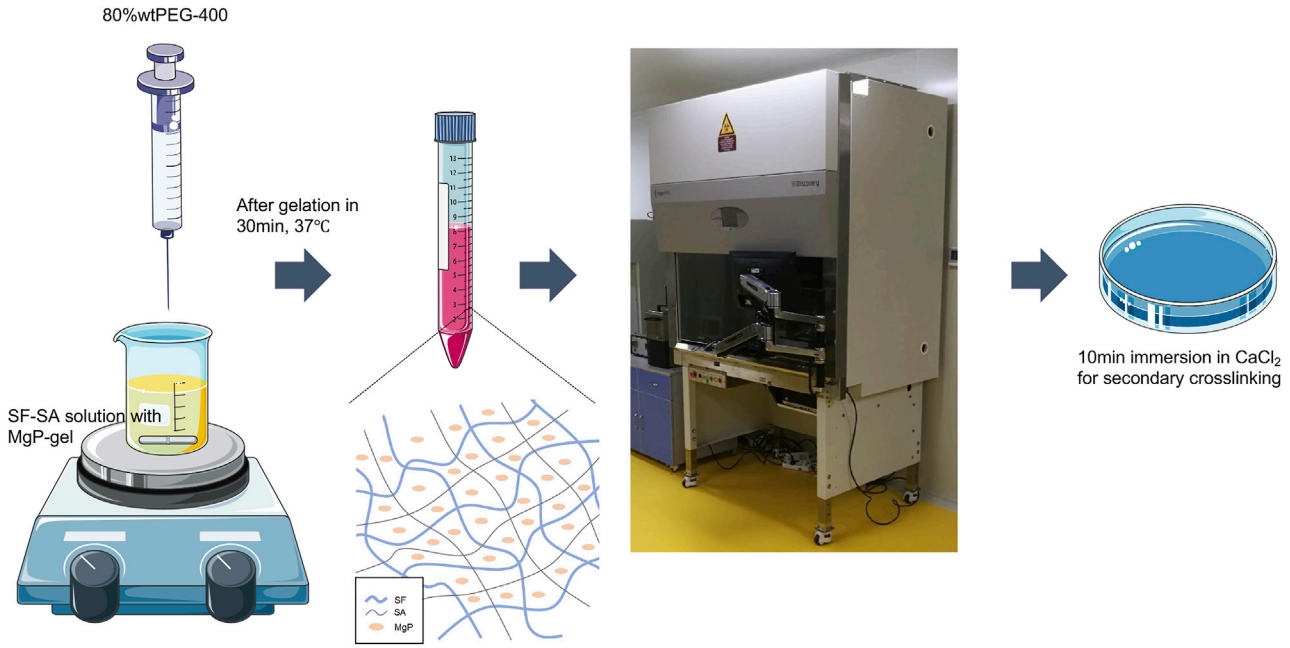

FIGURE 1 | The flow chart is an illustration of how the SF-SA and SF-SA/MgP hydrogel scaffolds were fabricated. The whole process was in a sterilized environment.

2.2.4.4 Alkaline Phosphatase Activity

To measure alkaline phosphatase activity, BMSCs were plated in 24-well culture plates (2×10^4 cells/mL) with osteogenic differentiation medium (ODM). To be detailed, the ODM was a mixture of 100 μM dexamethasone (Sigma-Aldrich), 10 mM β-glycerophosphate (Sigma-Aldrich), and 50 μM ascorbate-2-phosphate (Sigma-Aldrich) with the DMEM medium. To avoid the interference from silk fibroin protein in the extraction of cell proteins, the ODM used in this section was further prepared according to the International Organization for Standardization (ISO)-10993-5. Specifically, hydrogel films were immersed in ODM for 24 h before the extracts of the hydrogel were filtrated for cell culturing. After the cells were cultured in ODM for 7 days, the cells were washed with PBS 3 times before being lysed in 200 μL 0.1% Triton X-100 on ice for 10 min. Afterward, the ALP activity was evaluated colorimetrically with the Alkaline Phosphatase Assay Kit (P0321, Beyotime Biotechnology, China). The optical density (λ = 405 nm) was analyzed by using a microplate reader (SpectraMaxM2e, MD). Staining of ALP enzyme was also performed by a BCIP/NBT alkaline phosphatase color development kit (Beyotime, China) for visualization.

2.2.5 Fabrication of 3D Silk Fibroin and Sodium Alginate and SF-SA/MgP Hydrogel Scaffolds

The selected ratio of SF-SA/MgP was based on the cell proliferation and early osteodifferentiation performance of three hybrid SF-SA/MgP hydrogel films. To fabricate the 3D scaffold with the MgP-based hydrogel bioink, the final chosen concentration of M2.5 (SF-SA/MgP with the concentration of MgP 2.5%wt), and M0 hydrogel (SF-SA) was set as the control group. The fabrication was performed using a 3D printing system (3D Discovery, regenHU, Switzerland), and the whole fabrication process is shown in **Figure 1**. The diameter of the applied single nozzle was 510 μm and the moving speed was set as 6 mm/s, the pneumatic pressure was configured at 100 kPa. When the process of printing was finished, the structures were further cross-linked by immersion in 0.2 M $CaCl_2$ to maintain outside shape and enhance structural stability. At last, the structure was washed with PBS 3 times to exclude PEG and Cl^- ions.

2.2.6 Scanning Electron Microscopy

The morphology of all hydrogel scaffolds was investigated using scanning electron microscopy (MAIA3 TESCAN). All the hydrogel scaffolds were pre-lyophilized and coated with palladium prior to SEM observation.

2.2.7 Analysis of Osteodifferentiation on 3D Hydrogel Structures

Alizarin Red S staining of the scaffolds was carried out to analyze calcium mineralization. The scaffolds were washed twice with PBS and then fixed in 4% paraformaldehyde. After fixing for 30 min, all samples were washed again with PBS 3 times. Then 0.2% Alizarin Red S (Shanghaiyuanye Bio-Technology Co., Ltd., China) was added to react with calcium nodules for 5 min. The stained samples were then rinsed with PBS until the remaining red dye was completely removed. The optical images of the samples were captured by a stereomicroscope. To qualify the calcium mineral density, the obtained optical density (λ = 562 nm) was measured by a microplate reader after the stained samples were lysed with 10% cetylpyridinium chloride (CPC) dissolved in ddH_2O for 1 h.

TABLE 2 | Primer sequences used for this study.

Gene	Primer Pairs	Primer Sequence (5′-3′)
ALP	Forward	aacatcagggacattgacgtg
	Reverse	gtatctcggtttgaagctcttcc
OPN	Forward	atgatggccgaggtgatagt
	Reverse	accattcaactcctcgcttt
OCN	Forward	agcaaaggtgcagcctttgt
	Reverse	gcgcctgggtctcttcact
GAPDH	Forward	gcaccgtcaaggctgagaac
	Reverse	tggtgaagacgccagtgga

A quantitative real-time polymerase chain reaction (RT-PCR) for the BMSCs co-culture with hydrogel scaffolds was conducted on day 7 and day 14, to measure the relative gene expression levels of alkaline phosphatase (ALP), osteocalcin (OCN), and osteopontin (OPN) (Primer sequence showed in **Table 2**). The normalized housekeeping gene was Glyceraldehyde-3-phosphatedehydrogenase (GAPDH). RNA isolation was performed with Takara minibest universal RNA extraction kit and then cDNA was synthesized by PrimeScript RT Master Mix (Perfect Real Time) (Takara, Japan). The RT-PCR was performed by QuantStudio™ 6 and 7 Flex Real-Time PCR Systems (Applied Biosystems, United States) and the TB Green Premix Ex Taq II (Takara, Japan) following the manufacturer's protocols. All reactions were run in quintuplicate for each sample and each gene.

2.3 Statistical Analysis

All obtained data was used processed and analyzed with OriginPro 8 (OriginLab) and Prism 9 (GraphPad) for statistical analyses. ANOVA analysis of variance test was applied in this study based on the number of variables, and comparison between groups was with Turkey test. In all the analyses, $p < 0.05$ was considered statistically significant ($^{*}p < 0.05$, $^{**}p < 0.01$, $^{****}p < 0.0001$).

3 RESULTS

3.1 Scaffold Characterization

Fourier transform infrared (FT-IR) spectroscopy was applied to observe the material properties by analyzing specific absorption peaks to determine the structure of organic compounds in lyophilized SF-SA and SF-SA/MgP particles. As the **Figure 2A** illustrated, all the samples showed specific peaks at 1,634 cm^{-1} (alkyl C-H stretching vibrations), 1,528 cm^{-1}, corresponding to bending vibration of amide nitrogen and hydrogen, and the carbonyl group of carboxy anion after carboxylic acid salt was also peaked near this region, proving the presence of β-sheet in silk fibroin (Kweon et al., 2001). Peaks at 1,460 and 1,353 cm^{-1} corresponded to alkyl C-H bending vibration, 1,249 cm^{-1} to carbon-nitrogen stretching vibration, and 1,103 cm^{-1} to C-O-C stretching vibration. In addition, a broad peak at 3,416 cm^{-1} corresponded to amino and O-H stretching vibration (the area with hydrogen bond was broad), and peaks at 948 cm^{-1} and 840 cm^{-1} were fingerprint areas of organic materials, revealing the presence of $(HPO_4)^{2-}$ (Chen et al., 2018). Overall, with an increased concentration of MgP, the infrared spectra deviation in M1 and M2.5 was not as significant as that in M3, illustrating that the transformation of β-sheet was not obliviously affected by the mixture in M1 and M2.5. In all MgP-added groups, the absorption peak of phosphate between 1,200 and 1,000 cm^{-1} (Vivekanandan et al., 1997; Zhang and Darvell, 2010; Yu et al., 2013) was very weak, presumably overlapped by the ether bond of organic materials.

3.2 Rheological

To determine the effect of MgP made on the rheological property of the hydrogel bioink, M0, M1, M2.5, and M3 were prepared only with PEG gelation. As the results showed in **Figure 2B**, the increasing content of MgP promoted the shear-thinning under a high-speed shear. Notably, the addition of magnesium phosphate increased the static viscosity of the material at the beginning. When the material was subjected to shearing, the shear viscosity of the material with MgP decreased more. Next, as the shear rate increased, this shear thinning effect is further enhanced. The relationship between the storage modulus (G′) and loss modulus (G″) of the four samples is shown in **Figure 2C**. In the frequency ranging from 0.1 to 10 Hz, all samples were basically in line with G′> G″, proving that the material in this frequency range was a viscoelastic solid material. From low frequency to high frequency, the storage modulus change curve of the four materials was stable and slightly increased when the frequency is under 10 Hz. In the dynamic modulus of the four samples, the hydrogels with MgP were higher, and the loss modulus was M2.5 > M1 > M3 > M0 as shown.

3.3 Cell Proliferation and Viability

Figure 3A showed the evolution of the BMSCs proliferation performed by a CCK-8 assay (displayed as mean OD value) over 7 days. The average cell viability in the former three experimental groups was not significantly different from the control group in the first 3 days, suggesting that the chemical compositions of the hydrogels were cytocompatible with BMSCs at an early stage. At the interval time of day 5, the proliferation of BMSC on hydrogel films was slightly lower than in the control group but there was no significant difference among the four experimental groups. On day 7, The proliferation result of M2.5 was superior than other hydrogel groups but was still lower than control. Notably, for groups M0, M1, and M2.5, the lower cell viability in hydrogel films can be explained by the fragile construction of films and the degradation of hydrogels. For M3, however, an overdosed MgP content may be unbeneficial for cell proliferation because of an excessive release of Mg^{2+} or rapid degradation of hydrogel films. Additionally, the successive refreshment of the culture medium through aspiration and the washing procedure may also result in a decrease in the cell number.

In fluorescence microscopy images, the BMSCs adhesion on hydrogel films was the cells seeded on days 3 and 7. The F-actin filaments of the cell cytoskeleton and cell nuclei were stained with phalloidin (red) and DAPI (blue), respectively. **Figures 3B–E**

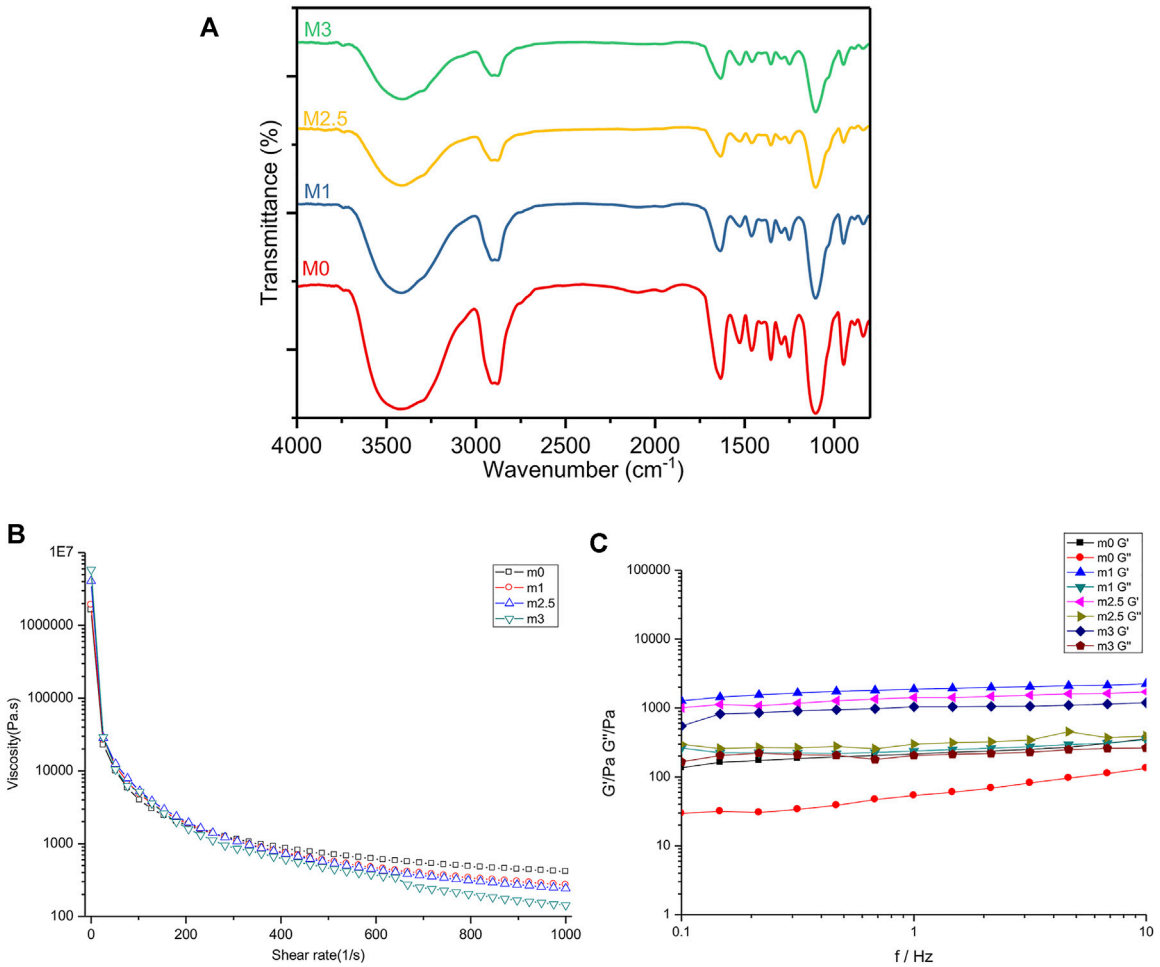

FIGURE 2 | Mechanical characteristics of m0, m1, m2.5, and m3 hydrogels. **(A)** FT-IR spectra of four films after lyophilization. **(B,C)** rheological analyses of four hydrogels before crosslinking with $CaCl_2$. **(B)** flow curves of hybrid bioinks with a shear rate from 0.1% to 100%. **(C)** G′ and G″ of four hydrogels under the mode of frequency sweep ranging from 0.1 to 10 Hz.

confirmed that the cells on the M2.5 and M3 scaffold tended to form cell aggregates and a non-uniform distribution on the films (**Figures 3D,E**), whereas BMSCs seeded on M0 and M1 (**Figures 3B,C**) showed a more homogeneous distribution on day 3. When it comes to day 7, BMCs on four scaffolds (**Figures 3B–E**) all displayed uniform distribution with a high cell density, proving that the surfaces of four kinds of hydrogel films all presented to be positive for cell adhesion and viability.

3.4 Alp Activity

The ALP expression is a key characteristic of osteogenic differentiation in the early stage of cell differentiation, reflecting the ability of osteoblasts to synthesize collagen I and to form a bone matrix (Basdra and Komposch, 1997). On day 7, the cells in a 24-well-plate induced by the extracts of four hydrogels were stained with a BCIP/NBT alkaline phosphatase color development kit. As **Figures 4A–H** showed, the M2.5 and M3 groups had deeper colors than M0 and M1 groups. **Figure 3I** showed the ALP activity on the same plate. The difference in ALP activity between the low content of MgP and high MgP content groups was significant ($p < 0.05$). The ALP activity of the M2.5 was the highest reaching 12.49 U/gprot and M3 reaches to12.20 U/gprot. Both the high content MgP groups were showing significantly higher alp activities than M0 and M1 groups, where the value was only 4.49 U/gprot and 8.54 U/gprot, respectively.

3.5 Scanning Electron Microscope

The stereomicroscope and SEM images of the fabricated SF-SA and SF-SA/MgP scaffolds were shown in **Figure 5A,B**. In stereomicroscope, the surface of SF-SA was smoother and more uniform. On the contrary, in SEM images, the micro-pores of SF-SA/MgP were more homogeneous and evenly distributed, as the average micro-pores diameter was around 57.885 ± 5.341 μm while the pore size in SF-SA ranged from 31.25 to 88.18 μm. The energy spectrum (**Figure 5E–I** of SF-SA/MgP also showed that the elements of Ca, Na, P, and Mg were evenly distributed on the surface of

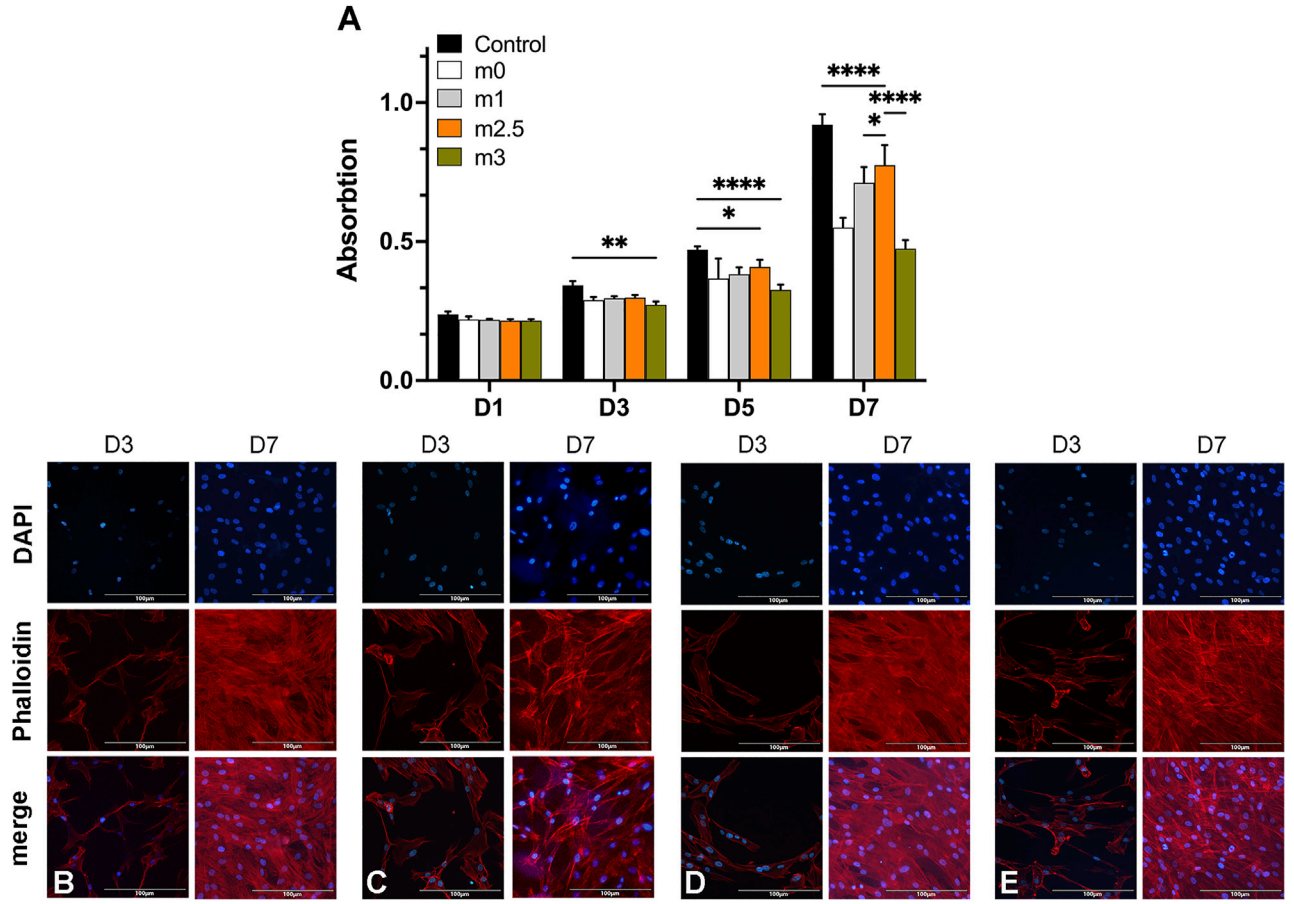

FIGURE 3 | (A) CCK8 assay of BMSCs on 2D hydrogel films at different time intervals (Day 1, 3, 5, and 7). **(B–E)** cells on films stained with DAPI (blue) and phalloidin (red) on day 3 and day 7.

scaffolds, proving that nano MgP particles were homogeneously distributed in the hydrogel scaffold. Moreover, a step-by-step crosslinking process in fabrication maintained its good injectability first during 3D printing, and further prevented the solid-liquid separation after immersion in $CaCl_2$.

3.6 Osteodifferentiation on 3D Hydrogel Structures

Figure 6A demonstrated the results of calcium deposition/mineralization by staining with alizarin red on day 14. As shown in the figure, the color of alizarin red was deeper as a result of the mixture of MgP. The quantification results were illustrated in **Figure 6B** where the OD values of SF-SA/MgP hydrogel were significantly higher, in correspondence with the staining results and previous alp activity analysis. For rt-PCR, **Figures 6C–E** showed the expression level of the osteogenic genes ALP, OCN, and OPN on day 7 and day 14. The gene expression of cells seeded on SF-SA/MgP scaffolds all presented higher levels than on SF-SA scaffolds, indicating that the osteogenic differentiation process of BMSCs on scaffolds was affected by the MgP component.

4 DISCUSSION

In our previous study, we designed an injectable silk-MgP hydrogel for the repair of the defect in bone tissues. However, in follow-up experiments we found that this kind of injectable hydrogel was seriously stuck with the loading plate of the 3D-print machine, making it impossible for a pre-designed scaffold to be fabricated and defect repaired. To overcome this issue, we made improvements by adding a low concentration of sodium alginate, with which we were able to fabricate a hydrogel bioink that can be applied for an extrusion 3D-print system.

In this newly hydrogel bioink, SF was the main component for the fabrication of the scaffold as SF is a natural polymer with excellent biocompatibility that can mimic the function of extracellular materials. There have been many reports on the successful application of SF-made 3D-printed scaffolds (Zhong et al., 2019; Kim et al., 2021a; Kim et al., 2021b).

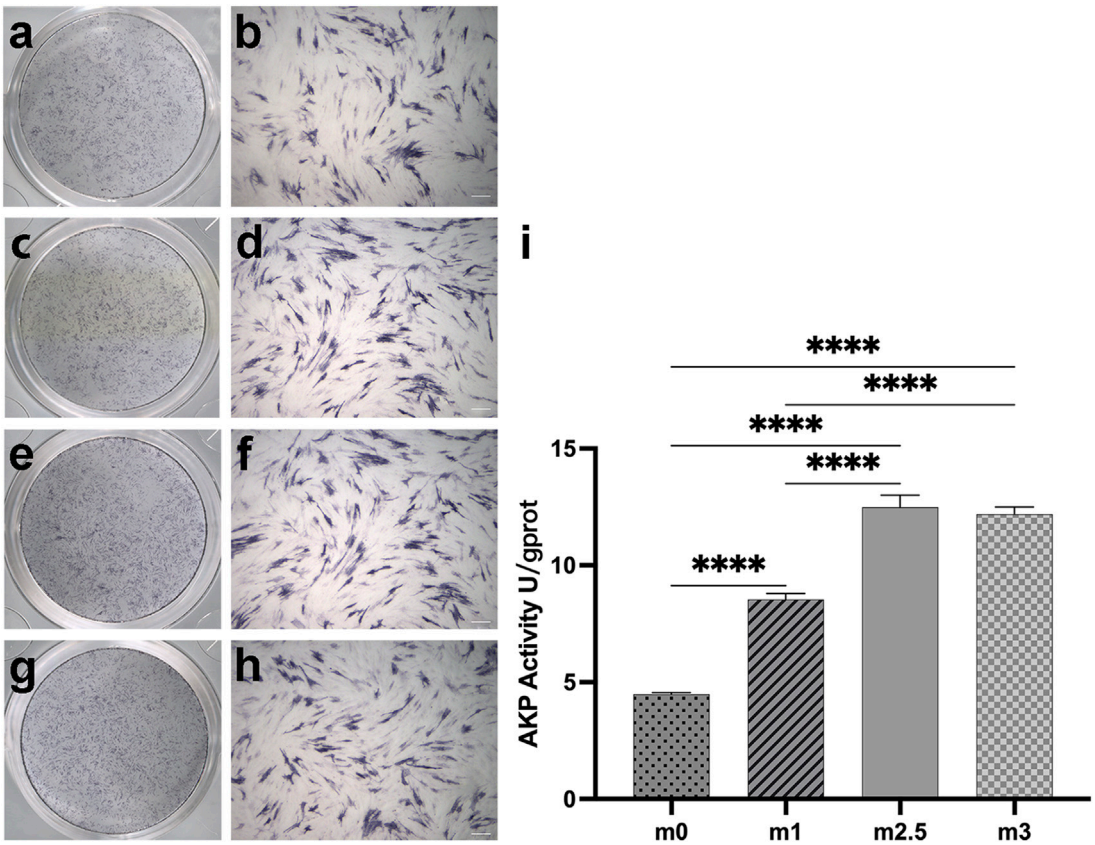

FIGURE 4 | (A–H): alp staining pictures after 7 days of cell culture, M0 **(A,B)**, M1 **(C,D)**, M2.5 **(E,F)**, and M3 **(G,H)** under scanning and 10× microscope. **(I)** the different alp activities in quantitative. Scale bar for 200 μm.

Theoretically, the silk protein can be catalytically hydrolyzed into amino acids under the action of proteolytic enzymes, then those amino acids would be metabolized by the body (Zheng et al., 2018). A recent study also revealed that the addition of sodium alginate can regulate the degradation rate of SF (Wang et al., 2020). The intermolecular covalent bonds and hydrogen bonds of SA macromolecule help SA form an interactive polymer network structure with SF which can affect the amount of silk II in SF hydrogel (Wang et al., 2020). In the following stage, the printed scaffold would be soaked into 0.2 M $CaCl_2$ to further reinforce the scaffold and better maintain its stability (Hua et al., 2010; Hong et al., 2016). The selection of 0.5%wt of SA is based on the fact that the transition of silk fibroin molecular in the follow-up experiments would not be affected while the viscosity of the SF solution was improved in this concentration, which is beneficial for the dispersion of MgP nanoparticles.

A thixotropic magnesium phosphate was also applied in this study in the form of nanoparticles instead of the traditional inorganic MgP particles. Laurenti, et al. were the first research group to study the fabrication and application of magnesium phosphate-based gel in bone repair (Laurenti et al., 2016). The MgP nanoparticles can evenly spread in the solution as a result of the ionization; the positive and negative charges simultaneously present lead to electrostatic and van der Waals interactions (Roth and Lenhoff, 1995). The particles dispersed in the solution, forming a 3D network known as the "house of cards" structure. (Barnes, 1997; Mewis and Wagner, 2009). By applying mechanical forces, thixotropic materials can be liquefied to flow; when the mechanical stress stops, the particles were driven into contact by Brownian motion to reform the 3D network again and the liquid-like dispersion is converted to solid-like gel. (Mewis and Wagner, 2009; Bergaya and Lagaly, 2013).

Generally, the hybrid hydrogel was confirmed to be a satisfying bioink for 3D scaffold production. The FT-IR spectrum of four hydrogel films shared similar structures with no obvious deviation, illustrating that the amount of MgP nanoparticles would not affect the transformation to the β-sheet in the SF solution. The absorption bands at a frequency ranging from 1,620 to 1,640 cm^{-1} and 1,695 to 1700 cm^{-1} corresponded to the functional groups in silk II form (Hu et al., 2006). As **Figure 2A** showed, the peaks at 1,634 cm^{-1} represented the existence of β-sheet structure (Kweon et al., 2001), but the value of transmittances decreased as the amount of the MgP increased.

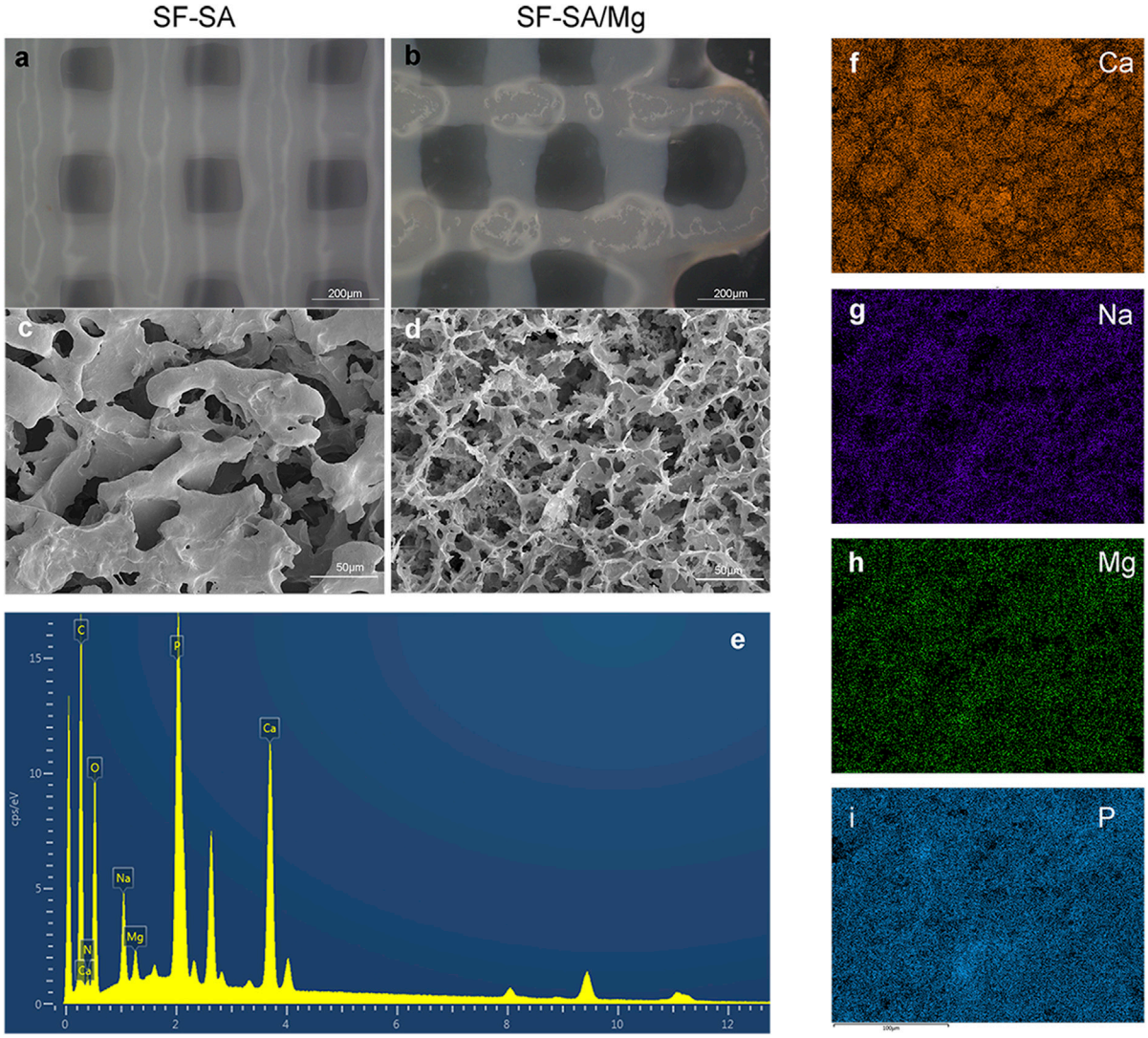

FIGURE 5 | Images of 3D-printed SF-SA **(A)** and SF-SA/MgP **(B)** scaffolds under stereoscopy, SEM images of the surface morphology of SF-SA **(C)** hydrogel and SF-SA/MgP **(D)** scaffolds. **(E–I)**: the surface of EDS of SF-SA/MgP scaffold.

For rheological analysis, an ideal substance for extrusion-based 3D printing should be shear-thinning, thixotropic, easily extruded, and with fine formability (Chung et al., 2013; Schuurman et al., 2013; Ozbolat and Hospodiuk, 2016). The four hydrogels in our study all showed well shear-thinning properties. The G' value was higher than that of G'' in frequency sweep mode in all samples, showing that the G' and G'' were independent of the change in frequency. This result indicated the gel-like behavior and a stable decentralized system of the bio-ink (Malkin et al., 2004).

To study the biocompatibility and bioactivity of the components in the hydrogel, MSCs were first seeded on 2D hydrogel films for cell viability and then incubated with extractions of biomaterials for ALP activity because the hydrogel films would collapse after 5 days due to the swelling of hydrogel. As shown in **Figure 3**, the CCK-8 analysis was in contradiction with the fluorescent staining. The decreased OD value in M3 on day 7 can be explained by the crack of hydrogel and washing with PBS. The extractions of hydrogels contained the releasing of Mg^{2+} with different concentrations; the results of CCK-8 and ALP activity exquisitely reflected the proper concentration of MgP which optimally promoted the osteogenic activity. The results of proliferation analysis and ALP activity were in accordance with a previous study (Wang et al., 2017), which revealed that low Mg^{2+} concentration (i.e., 0.1×10^{-3} M) had an inhibitory effect on the differentiation of

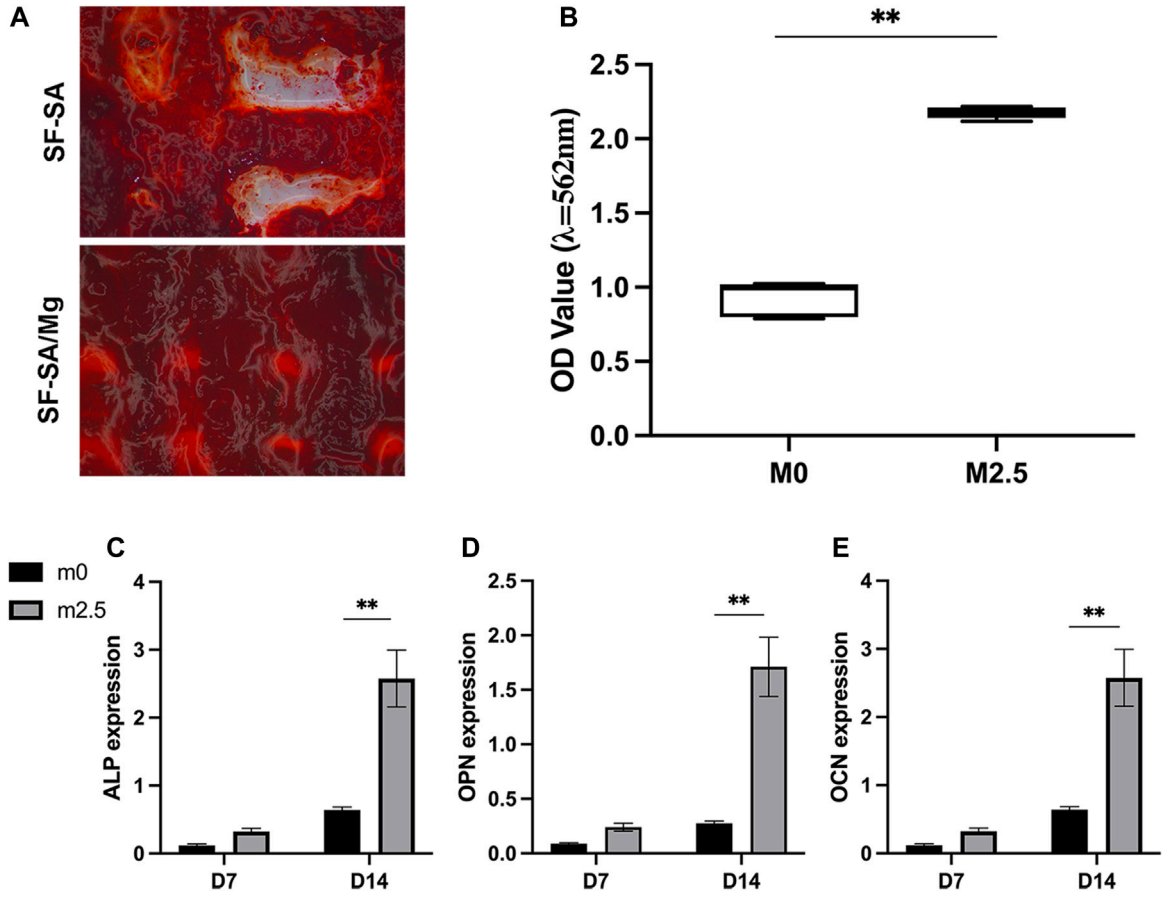

FIGURE 6 | 3D structures of SF-SA and SF-SA/MgP hydrogel scaffolds co-cultured with BMSCs on day 14. Alizarin staining **(A)**, and qualification by 10% CPC **(B)**. ALP, OCN, and OPN expression of each sample on days 7 and 14 **(C–E)**.

osteoblasts while an overdosed Mg^{2+} concentration (i.e., 18×10^{-3} M) was harmful to osseous metabolism (Basdra and Komposch, 1997; Wang et al., 2017).

In the process of the 3D scaffold fabrication, the air pressure was set at 100kPa, far less than the 0.45 MPa as described by Andrew C Daly, et al (Daly et al., 2016b). **Figures 5A,B** showed the shape fidelity and accuracy of the scaffold, reflected by the bar width and smoothness after the 4-layer printing. The SF-SA scaffold had a smoother surface but wider line than the SF-SA/MgP scaffold since SF-SA/MgP bio-ink had better recovery. The diameter of the syringe was finally set at 510 μm because the MgP nanoparticles would clog and block the finer syringe. This may be explained by the uneven gelation of the hydrogel. To overcome this problem, several improvements were proposed, such as the extension of stirring, ultrasonic, and syringe replacement with a conical nozzle. However, no feasible and sustainable solution had been found. Micro morphology of the scaffolds under SEM (**Figure 5C,D**) showed that the micropores of SF-SA/MgP were better for the medium penetration and absorption, as well as cell migration and adhesion. The results also explained why the performance of cell proliferation on M2.5 suppressed the performance on M0 because the M0 film had a smoother surface and more unevenly distributed micropores, making it difficult for cell attachment especially when the cell confluency reached over 80%.

5 CONCLUSION

The combination of MgP-based gel with silk fibroin and a low concentration of sodium alginate has been shown in previous research to be a highly effective hybrid hydrogel for 3D printing. We constructed an SF-SA/MgP hydrogel scaffold for bone tissue engineering with a content of 2.5% MgP. This hydrogel scaffold had good porosity with macro-pores around 200 μm between bars and outstanding biochemical properties that are beneficial to the growth of BMSCs. The mean diameter of micro-pores was 57.885 ± 5.341 μm. Moreover, as a bioactive hydrogel, it positively stimulated the osteogenic activity of cells due to the release of Mg^{2+}. Although the softness of SF-SA/MgP hydrogel can provide a microenvironment similar to ECM to use as cell-loaded bioink, it cannot be applied in force-loading structures like mandibular. The absence of experiments *in vivo* cannot explain the relationship between osteogenesis and degradation in detail.

Overall, this 3D-printing SF-SA/MgP hydrogel provides a potential solution to the bone defect issue and has the potential to be put into practice in future bone tissue engineering.

DATA AVAILABILITY STATEMENT

The datasets presented in this study can be found in online repositories. The names of the repository/repositories and accession number(s) can be found below: https://www.ncbi.nlm.nih.gov/genbank/, MK061162 https://www.ncbi.nlm.nih.gov/genbank/, HQ234608.1 https://www.ncbi.nlm.nih.gov/genbank/, AY663810.1 https://www.ncbi.nlm.nih.gov/genbank/, KY418007.1.

ETHICS STATEMENT

The animal study was reviewed and approved by the Animal Ethical and Welfare Committee of Nanjing Medical University.

AUTHOR CONTRIBUTIONS

QM and SB contributed to the conception and design of the study. QM conducted the experiments mentioned in the manuscript. QM performed the statistical analysis and wrote the first draft of the manuscript. BZ and HZ wrote sections of the manuscript. SB is in charge of proofreading and revising the manuscript. All authors contributed to manuscript revision, read, and approved the submitted version.

FUNDING

The study is kindly funded by the National Natural Science Foundation of China (81670967) and the Jiangsu Provincial Department of Health (H201504).

REFERENCES

Babaie, E., Lin, B., and Bhaduri, S. B. (2017). A New Method to Produce Macroporous Mg-Phosphate Bone Growth Substitutes. *Mater. Sci. Eng. C* 75, 602–609. doi:10.1016/j.msec.2017.02.111

Babaie, E., Lin, B., Goel, V. K., and Bhaduri, S. B. (2016). Evaluation of Amorphous Magnesium Phosphate (AMP) Based Non-Exothermic Orthopedic Cements. *Biomed. Mat.* 11 (5), 055010. doi:10.1088/1748-6041/11/5/055010

Barnes, H. A. (1997). Thixotropy—A Review. *J. Newt. Fluid Mech.* 70 (1), 1–33. doi:10.1016/s0377-0257(97)00004-9

Basdra, E. K., and Komposch, G. (1997). Osteoblast-Like Properties of Human Periodontal Ligament Cells: An *In Vitro* Analysis. *Eur. J. Orthod.* 19 (6), 615–621. doi:10.1093/ejo/19.6.615

Bergaya, F., and Lagaly, G. (2013). *Handbook of Clay Science*. Oxford: Newnes.

Cao, Y., and Wang, B. (2009). Biodegradation of Silk Biomaterials. *Int. J. Mol. Sci.* 10 (4), 1514–1524. doi:10.3390/ijms10041514

Chen, Y., Wang, Y., Yang, Q., Liao, Y., Zhu, B., Zhao, G., et al. (2018). A Novel Thixotropic Magnesium Phosphate-Based Bioink with Excellent Printability for Application in 3D Printing. *J. Mat. Chem. B* 6 (27), 4502–4513. doi:10.1039/c8tb01196f

Chen, Y., Xiong, X., Liu, X., Cui, R., Wang, C., Zhao, G., et al. (2020). 3D Bioprinting of Shear-Thinning Hybrid Bioinks with Excellent Bioactivity Derived from Gellan/Alginate and Thixotropic Magnesium Phosphate-Based Gels. *J. Mat. Chem. B* 8 (25), 5500–5514. doi:10.1039/d0tb00060d

Chung, J. H. Y., Naficy, S., Yue, Z., Kapsa, R., Quigley, A., Moulton, S. E., et al. (2013). Bio-ink Properties and Printability for Extrusion Printing Living Cells. *Biomater. Sci.* 1 (7), 763–773. doi:10.1039/c3bm00012e

Daly, A. C., Critchley, S. E., Rencsok, E. M., and Kelly, D. J. (2016). A Comparison of Different Bioinks for 3D Bioprinting of Fibrocartilage and Hyaline Cartilage. *Biofabrication* 8 (4), 045002. doi:10.1088/1758-5090/8/4/045002

Daly, A. C., Cunniffe, G. M., Sathy, B. N., Jeon, O., Alsberg, E., and Kelly, D. J. (2016). 3D Bioprinting of Developmentally Inspired Templates for Whole Bone Organ Engineering. *Adv. Healthc. Mat.* 5 (18), 2353–2362. doi:10.1002/adhm.201600182

de Moraes, M. A., Silva, M. F., Weska, R. F., and Beppu, M. M. (2014). Silk Fibroin and Sodium Alginate Blend: Miscibility and Physical Characteristics. *Mater. Sci. Eng. C* 40, 85–91. doi:10.1016/j.msec.2014.03.047

Du, X., Wei, D., Huang, L., Zhu, M., Zhang, Y., and Zhu, Y. (2019). 3D Printing of Mesoporous Bioactive Glass/Silk Fibroin Composite Scaffolds for Bone Tissue Engineering. *Mater. Sci. Eng. C* 103, 109731. doi:10.1016/j.msec.2019.05.016

Gong, X., Branford-White, C., Tao, L., Li, S., Quan, J., Nie, H., et al. (2016). Preparation and Characterization of a Novel Sodium Alginate Incorporated Self-Assembled Fmoc-FF Composite Hydrogel. *Mater. Sci. Eng. C* 58, 478–486. doi:10.1016/j.msec.2015.08.059

Groll, J., Boland, T., Blunk, T., Burdick, J. A., Cho, D.-W., Dalton, P. D., et al. (2016). Biofabrication: Reappraising the Definition of an Evolving Field. *Biofabrication* 8 (1), 013001. doi:10.1088/1758-5090/8/1/013001

Gudapati, H., Dey, M., and Ozbolat, I. (2016). A Comprehensive Review on Droplet-Based Bioprinting: Past, Present and Future. *Biomaterials* 102, 20–42. doi:10.1016/j.biomaterials.2016.06.012

Hong, S. H., Shin, M., Lee, J., Ryu, J. H., Lee, S., Yang, J. W., et al. (2016). STAPLE: Stable Alginate Gel Prepared by Linkage Exchange from Ionic to Covalent Bonds. *Adv. Healthc. Mat.* 5 (1), 75–79. doi:10.1002/adhm.201400833

Hu, X., Kaplan, D., and Cebe, P. (2006). Determining Beta-Sheet Crystallinity in Fibrous Proteins by Thermal Analysis and Infrared Spectroscopy. *Macromolecules* 39 (18), 6161–6170. doi:10.1021/ma0610109

Hua, S., Ma, H., Li, X., Yang, H., and Wang, A. (2010). pH-Sensitive Sodium Alginate/Poly(Vinyl Alcohol) Hydrogel Beads Prepared by Combined Ca2+ Crosslinking and Freeze-Thawing Cycles for Controlled Release of Diclofenac Sodium. *Int. J. Biol. Macromol.* 46 (5), 517–523. doi:10.1016/j.ijbiomac.2010.03.004

Jiang, X., Zhao, J., Wang, S., Sun, X., Zhang, X., Chen, J., et al. (2009). Mandibular Repair in Rats with Premineralized Silk Scaffolds and BMP-2-Modified bMSCs. *Biomaterials* 30 (27), 4522–4532. doi:10.1016/j.biomaterials.2009.05.021

Kanter, B., Vikman, A., Brückner, T., Schamel, M., Gbureck, U., and Ignatius, A. (2018). Bone Regeneration Capacity of Magnesium Phosphate Cements in a Large Animal Model. *Acta Biomater.* 69, 352–361. doi:10.1016/j.actbio.2018.01.035

Kim, E., Seok, J. M., Bae, S. B., Park, S. A., and Park, W. H. (2021). Silk Fibroin Enhances Cytocompatibilty and Dimensional Stability of Alginate Hydrogels for Light-Based Three-Dimensional Bioprinting. *Biomacromolecules* 22 (5), 1921–1931. doi:10.1021/acs.biomac.1c00034

Kim, S. H., Hong, H., Ajiteru, O., Sultan, M. T., Lee, Y. J., Lee, J. S., et al. (2021). 3D Bioprinted Silk Fibroin Hydrogels for Tissue Engineering. *Nat. Protoc.* 16 (12), 5484–5532. doi:10.1038/s41596-021-00622-1

Kim, S. S., Utsunomiya, H., Koski, J. A., Wu, B. M., Cima, M. J., Sohn, J., et al. (1998). Survival and Function of Hepatocytes on a Novel Three-Dimensional Synthetic Biodegradable Polymer Scaffold with an Intrinsic Network of Channels. *Ann. Surg.* 228 (1), 8–13. doi:10.1097/00000658-199807000-00002

Klammert, U., Ignatius, A., Wolfram, U., Reuther, T., and Gbureck, U. (2011). *In Vivo* degradation of Low Temperature Calcium and Magnesium Phosphate Ceramics in a Heterotopic Model. *Acta Biomater.* 7 (9), 3469–3475. doi:10.1016/j.actbio.2011.05.022

Kweon, H., Ha, H. C., Um, I. C., and Park, Y. H. (2001). Physical Properties of Silk Fibroin/Chitosan Blend Films. *J. Appl. Polym. Sci.* 80 (7), 928–934. doi:10.1002/app.1172

Laurenti, M., Al Subaie, A., Abdallah, M.-N., Cortes, A. R. G., Ackerman, J. L., Vali, H., et al. (2016). Two-Dimensional Magnesium Phosphate Nanosheets Form

Highly Thixotropic Gels that Up-Regulate Bone Formation. *Nano Lett.* 16 (8), 4779–4787. doi:10.1021/acs.nanolett.6b00636

Lee, K. Y., and Mooney, D. J. (2012). Alginate: Properties and Biomedical Applications. *Prog. Polym. Sci.* 37 (1), 106–126. doi:10.1016/j.progpolymsci.2011.06.003

Ma, H., Feng, C., Chang, J., and Wu, C. (2018). 3D-Printed Bioceramic Scaffolds: From Bone Tissue Engineering to Tumor Therapy. *Acta Biomater.* 79, 37–59. doi:10.1016/j.actbio.2018.08.026

Malkin, A. Y., Masalova, I., Slatter, P., and Wilson, K. (2004). Effect of Droplet Size on the Rheological Properties of Highly-Concentrated w/o Emulsions. *Rheol. Acta* 43 (6), 584–591. doi:10.1007/s00397-003-0347-2

Markstedt, K., Mantas, A., Tournier, I., Martínez Ávila, H., Hägg, D., and Gatenholm, P. (2015). 3D Bioprinting Human Chondrocytes with Nanocellulose-Alginate Bioink for Cartilage Tissue Engineering Applications. *Biomacromolecules* 16 (5), 1489–1496. doi:10.1021/acs.biomac.5b00188

Mestres, G., and Ginebra, M.-P. (2011). Novel Magnesium Phosphate Cements with High Early Strength and Antibacterial Properties. *Acta Biomater.* 7 (4), 1853–1861. doi:10.1016/j.actbio.2010.12.008

Mewis, J., and Wagner, N. J. (2009). Thixotropy. *Adv. Colloid Interface Sci.* 147-148, 214–227. doi:10.1016/j.cis.2008.09.005

Murphy, S. V., and Atala, A. (2014). 3D Bioprinting of Tissues and Organs. *Nat. Biotechnol.* 32 (8), 773–785. doi:10.1038/nbt.2958

Nabiyouni, M., Brückner, T., Zhou, H., Gbureck, U., and Bhaduri, S. B. (2018). Magnesium-Based Bioceramics in Orthopedic Applications. *Acta Biomater.* 66, 23–43. doi:10.1016/j.actbio.2017.11.033

Ostrowski, N., Roy, A., and Kumta, P. N. (2016). Magnesium Phosphate Cement Systems for Hard Tissue Applications: A Review. *ACS Biomater. Sci. Eng.* 2 (7), 1067–1083. doi:10.1021/acsbiomaterials.6b00056

Ozbolat, I. T., and Hospodiuk, M. (2016). Current Advances and Future Perspectives in Extrusion-Based Bioprinting. *Biomaterials* 76, 321–343. doi:10.1016/j.biomaterials.2015.10.076

Parak, A., Pradeep, P., du Toit, L. C., Kumar, P., Choonara, Y. E., and Pillay, V. (2019). Functionalizing Bioinks for 3D Bioprinting Applications. *Drug Discov. Today* 24 (1), 198–205. doi:10.1016/j.drudis.2018.09.012

Pei, P., Qi, X., Du, X., Zhu, M., Zhao, S., and Zhu, Y. (2016). Three-Dimensional Printing of Tricalcium Silicate/Mesoporous Bioactive Glass Cement Scaffolds for Bone Regeneration. *J. Mat. Chem. B* 4 (46), 7452–7463. doi:10.1039/c6tb02055k

Placone, J. K., and Engler, A. J. (2018). Recent Advances in Extrusion-Based 3D Printing for Biomedical Applications. *Adv. Healthc. Mater* 7 (8), e1701161. doi:10.1002/adhm.201701161

Roth, C. M., and Lenhoff, A. M. (1995). Electrostatic and van der Waals Contributions to Protein Adsorption: Comparison of Theory and Experiment. *Langmuir* 11 (9), 3500–3509. doi:10.1021/la00009a036

Saunders, R. E., and Derby, B. (2014). Inkjet Printing Biomaterials for Tissue Engineering: Bioprinting. *Int. Mater. Rev.* 59 (8), 430–448. doi:10.1179/1743280414y.0000000040

Schuurman, W., Levett, P. A., Pot, M. W., van Weeren, P. R., Dhert, W. J. A., Hutmacher, D. W., et al. (2013). Gelatin-methacrylamide Hydrogels as Potential Biomaterials for Fabrication of Tissue-Engineered Cartilage Constructs. *Macromol. Biosci.* 13 (5), 551–561. doi:10.1002/mabi.201200471

Shi, W., Sun, M., Hu, X., Ren, B., Cheng, J., Li, C., et al. (2017). Structurally and Functionally Optimized Silk-Fibroin-Gelatin Scaffold Using 3D Printing to Repair Cartilage Injury *In Vitro* and *In Vivo*. *Adv. Mater* 29 (29), 1701089. doi:10.1002/adma.201701089

Smrdel, P., Bogataj, M., Podlogar, F., Planinšek, O., Zajc, N., Mazaj, M., et al. (2006). Characterization of Calcium Alginate Beads Containing Structurally Similar Drugs. *Drug Dev. Industrial Pharm.* 32 (5), 623–633. doi:10.1080/03639040600599863

Sorkio, A., Koch, L., Koivusalo, L., Deiwick, A., Miettinen, S., Chichkov, B., et al. (2018). Human Stem Cell Based Corneal Tissue Mimicking Structures Using Laser-Assisted 3D Bioprinting and Functional Bioinks. *Biomaterials* 171, 57–71. doi:10.1016/j.biomaterials.2018.04.034

Tamimi, F., Nihouannen, D. L., Bassett, D. C., Ibasco, S., Gbureck, U., Knowles, J., et al. (2011). Biocompatibility of Magnesium Phosphate Minerals and Their Stability under Physiological Conditions. *Acta Biomater.* 7 (6), 2678–2685. doi:10.1016/j.actbio.2011.02.007

Venkatesan, J., Bhatnagar, I., Manivasagan, P., Kang, K.-H., and Kim, S.-K. (2015). Alginate Composites for Bone Tissue Engineering: A Review. *Int. J. Biol. Macromol.* 72, 269–281. doi:10.1016/j.ijbiomac.2014.07.008

Vivekanandan, K., Selvasekarapandian, S., Kolandaivel, P., Sebastian, M. T., and Suma, S. (1997). Raman and FT-IR Spectroscopic Characterisation of Flux Grown KTiOPO4 and KRbTiOPO4 Non-Linear Optical Crystals. *Mater. Chem. Phys.* 49 (3), 204–210. doi:10.1016/s0254-0584(97)80165-4

Wang, J., Ma, X.-Y., Feng, Y.-F., Ma, Z.-S., Ma, T.-C., Zhang, Y., et al. (2017). Magnesium Ions Promote the Biological Behaviour of Rat Calvarial Osteoblasts by Activating the PI3K/Akt Signalling Pathway. *Biol. Trace Elem. Res.* 179 (2), 284–293. doi:10.1007/s12011-017-0948-8

Wang, X., Kluge, J. A., Leisk, G. G., and Kaplan, D. L. (2008). Sonication-Induced Gelation of Silk Fibroin for Cell Encapsulation. *Biomaterials* 29 (8), 1054–1064. doi:10.1016/j.biomaterials.2007.11.003

Wang, X., Partlow, B., Liu, J., Zheng, Z., Su, B., Wang, Y., et al. (2015). Injectable Silk-Polyethylene Glycol Hydrogels. *Acta Biomater.* 12, 51–61. doi:10.1016/j.actbio.2014.10.027

Wang, Y., Fan, S., Li, Y., Niu, C., Li, X., Guo, Y., et al. (2020). Silk Fibroin/Sodium Alginate Composite Porous Materials with Controllable Degradation. *Int. J. Biol. Macromol.* 150, 1314–1322. doi:10.1016/j.ijbiomac.2019.10.141

Yang, X., Xie, B., Wang, L., Qin, Y., Henneman, Z. J., and Nancollas, G. H. (2011). Influence of Magnesium Ions and Amino Acids on the Nucleation and Growth of Hydroxyapatite. *CrystEngComm* 13 (4), 1153–1158. doi:10.1039/c0ce00470g

Yu, H., Deng, D., Li, Y., Xu, S., Li, Y., Yu, C., et al. (2013). Electronic Structure and Luminescent Properties of Ca5(PO4)2(SiO4):Eu2+ Green-Emitting Phosphor for white Light Emitting Diodes. *Opt. Commun.* 289, 103–108. doi:10.1016/j.optcom.2012.09.069

Zhang, H., and Darvell, B. W. (2010). Synthesis and Characterization of Hydroxyapatite Whiskers by Hydrothermal Homogeneous Precipitation Using Acetamide. *Acta Biomater.* 6 (8), 3216–3222. doi:10.1016/j.actbio.2010.02.011

Zhang, J., Zhao, S., Zhu, Y., Huang, Y., Zhu, M., Tao, C., et al. (2014). Three-Dimensional Printing of Strontium-Containing Mesoporous Bioactive Glass Scaffolds for Bone Regeneration. *Acta Biomater.* 10 (5), 2269–2281. doi:10.1016/j.actbio.2014.01.001

Zhang, W., Wang, X., Wang, S., Zhao, J., Xu, L., Zhu, C., et al. (2011). The Use of Injectable Sonication-Induced Silk Hydrogel for VEGF165 and BMP-2 Delivery for Elevation of the Maxillary Sinus Floor. *Biomaterials* 32 (35), 9415–9424. doi:10.1016/j.biomaterials.2011.08.047

Zheng, A., Cao, L., Liu, Y., Wu, J., Zeng, D., Hu, L., et al. (2018). Biocompatible Silk/Calcium Silicate/Sodium Alginate Composite Scaffolds for Bone Tissue Engineering. *Carbohydr. Polym.* 199, 244–255. doi:10.1016/j.carbpol.2018.06.093

Zhong, N., Dong, T., Chen, Z., Guo, Y., Shao, Z., and Zhao, X. (2019). A Novel 3D-Printed Silk Fibroin-Based Scaffold Facilitates Tracheal Epithelium Proliferation *In Vitro*. *J. Biomater. Appl.* 34 (1), 3–11. doi:10.1177/0885328219845092

Conflict of Interest: The authors declare that the research was conducted in the absence of any commercial or financial relationships that could be construed as a potential conflict of interest.

Publisher's Note: All claims expressed in this article are solely those of the authors and do not necessarily represent those of their affiliated organizations, or those of the publisher, the editors, and the reviewers. Any product that may be evaluated in this article, or claim that may be made by its manufacturer, is not guaranteed or endorsed by the publisher.